PROCEEDINGS OF SPIE

SPIEDigitalLibrary.org/conference-proceedings-of-spie

On-chip infrared sensors: redefining the benefits of scaling

Derek Kita, Hongtao Lin, Anu Agarwal, Anupama Yadav, Kathleen Richardson, et al.

SPIE.

On-chip infrared sensors: redefining the benefits of scaling

Derek Kita[a], Hongtao Lin[a], Anu Agarwal[a], Anupama Yadav[b], Kathleen Richardson[b], Igor Luzinov[c], Tian Gu[a], Juejun Hu[a,*]

[a]Department of Materials Science and Engineering, Massachusetts Institute of Technology, Cambridge MA, 02139, USA; [b]College of Optics and Photonics, CREOL, University of Central Florida, Orlando, FL 32816, USA; [c]Department of Materials Science & Engineering, Clemson University, Clemson, SC 29634, USA

ABSTRACT

Infrared (IR) spectroscopy is widely recognized as a gold standard technique for chemical and biological analysis. Traditional IR spectroscopy relies on fragile bench-top instruments located in dedicated laboratory settings, and is thus not suitable for emerging field-deployed applications such as in-line industrial process control, environmental monitoring, and point-of-care diagnosis. Recent strides in photonic integration technologies provide a promising route towards enabling miniaturized, rugged platforms for IR spectroscopic analysis. It is therefore attempting to simply replace the bulky discrete optical elements used in conventional IR spectroscopy with their on-chip counterparts. This size down-scaling approach, however, cripples the system performance as both the sensitivity of spectroscopic sensors and spectral resolution of spectrometers scale with optical path length. In light of this challenge, we will discuss two novel photonic device designs uniquely capable of reaping performance benefits from microphotonic scaling. We leverage strong optical and thermal confinement in judiciously designed micro-cavities to circumvent the thermal diffusion and optical diffraction limits in conventional photothermal sensors and achieve a record 104 photothermal sensitivity enhancement. In the second example, an on-chip spectrometer design with the Fellgett's advantage is analyzed. The design enables sub-nm spectral resolution on a millimeter-sized, fully packaged chip without moving parts.

KEY WORDS: spectroscopy, optical sensors, optical resonators, photothermal effects, infrared sensors, chemical sensors

1. INTRODUCTION

Infrared spectroscopy probes the phonon vibrational states of molecules by measuring wavelength-dependent optical absorption in the mid-infrared regime (2-25 μm wavelength or 400-5,000 cm^{-1} in wave number). IR spectroscopy is widely recognized as the gold standard for chemical analysis given its superior specificity: molecular species can be uniquely identified with their characteristic optical absorption bands. Such a "fingerprinting" capability makes IR spectroscopy an ideal technology for applications involving chemical analysis in complex environments, such as industrial process control, environmental monitoring, food quality assessment, forensics, and remote sensing[1].

Traditional IR spectroscopy relies on bench-top instruments such as Fourier Transform Infrared (FTIR) spectrometers located in dedicated laboratories. These instruments are of the size of large desktop computers and easily cost over $100K. Further, robustness of these systems is often compromised by fragile mechanical moving parts or stringent optical alignment requirements. To meet the increasing demands of field-deployed applications, a number of portable

*hujuejun@mit.edu, phone: 1-302-766-3083.

Frontiers in Biological Detection: From Nanosensors to Systems IX, edited by Amos Danielli, Benjamin L. Miller, Sharon M. Weiss, Proc. of SPIE Vol. 10081, 100810F
 · doi: 10.1117/12.2250237

spectrometer products have been successfully developed by miniaturizing the discrete optical components used in their bench-top counterparts. The vast majority of these products, however, are designed for the visible and near-IR wavelengths (< 2 μm) where high-performance, low-cost photodetector arrays are readily available. Portable systems operating in the mid-IR range where the characteristic absorption bands of most molecules reside are still limited in terms of size, performance, and cost.

On-chip photonic integration offers an attractive solution to overcoming the aforementioned limitations associated with bench-top or current portable spectroscopic sensing systems. In addition to the apparent advantages in size, weight, and power (SWaP), no optical alignment is necessary between lithographically defined components in integrated photonic modules, thereby improving both manufacturing throughput and system ruggedness. Planar photonic integration further opens up the possibility of cost reduction leveraging standard high-volume semiconductor manufacturing processes for applications such as integration with consumer electronics.

The photonic integration approach also comes with its own pitfalls. In particular, on-chip sensors are often associated with an optical path length much smaller compared to their bulk counterparts. This is in part because of the small physical size of a chip, although the ultimate limit is imposed by optical propagation loss in integrated photonic components. Along this line, Section 2 analyzes performance evolution trends as sensor footprint reduces and points to key performance limitations arising from such size down-scaling. Sections 3 and 4 are then dedicated to two novel on-chip device designs capable of circumventing these limitations.

2. PERFORMANCE SCALING IN CHIP-SCALE SPECTROSCOPIC SENSING SYSTEMS

There are two basic system configurations for infrared spectroscopic sensing. In a "laser-scanning" sensing system, a tunable, narrow-line-width laser is coupled to a sensing element (e.g. waveguide evanescent sensors) where optical absorption by the analyte takes place. A single-element detector is used to record the spectrum as the laser wavelength is swept across the target spectral range. Alternatively, the "spectrometric" approach employs a broadband source in conjunction with a spectrometer to resolve the wavelength-dependent absorption in the sensing element. In this section, we show that key sensor performance metrics in both configurations (limit of detection in the former case and spectral resolution in the latter case) scale inversely with the effective optical path length. As a consequence, simple size down-scaling of conventional spectroscopic sensor designs to the chip-scale severely degrades the sensor performance often to an unacceptable level.

Assuming that the Lambert-Beer law holds across the entire analyte concentration range[3], optical absorbance of the analyte scales linearly with the target molecule concentration. In the following simple example, we assume a detector noise floor of 0.1% at some given sampling bandwidth, a molecular absorption cross section of 10^{-18} cm^2 (a typical value for molecules in the mid-infrared), that gas samples are held at 300 K and 1 atm, and that the detection limit corresponds to a signal-to-noise ratio (SNR) of unity. The limit of detection in terms of volumetric gas concentration in parts-per-million (ppm) is plotted as a function of optical path length in Fig. 1.

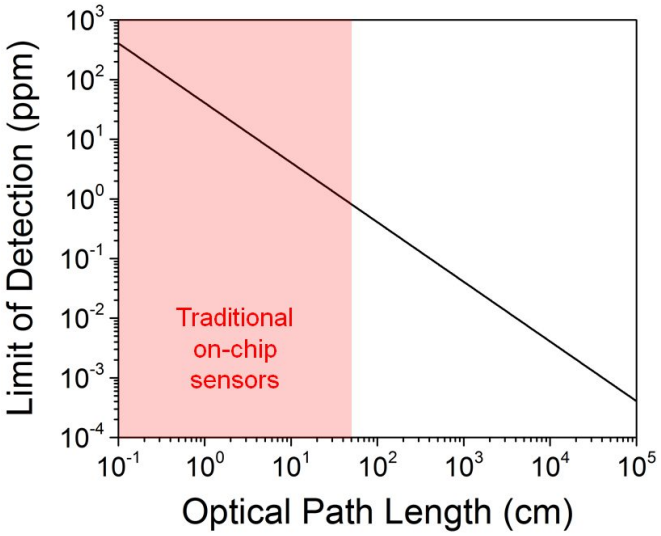

Fig. 1. Spectroscopic sensor limit of detection (in terms of volumetric gas concentration) as a function of optical path length, assuming a detector noise floor of 0.1% and a molecular absorption cross section of 10^{-18} cm^2.

Since propagation loss of on-chip optical waveguides is generally around 0.1 to a few dB/cm, the detection limit of traditional on-chip sensors is bound to the ppm level. We further note that using resonant cavity structures does not contribute to improving the limit of detection, since the effective optical path length in resonant cavities is similarly bound by optical propagation loss. The limited path length accounts for the vast performance gap between on-chip infrared spectroscopic sensors and free-space absorption cells (e.g. Herriott cells[4]), as the latter can achieve optical path lengths exceeding hundreds of meters and hence ppb-level detection.

On the other hand, compared to laser-scanning systems, spectrometric sensors claim the advantages of broad spectral bandwidth not limited by the gain spectrum of laser media, and are thus particularly suited for chemical analysis in a complex environment.

Fig. 2 illustrates two types of spectrometer configurations. In both configurations, a single-spatial-mode polychromatic optical input is launched into a generic linear and source-free optical system, which is characterized by a spatial distribution of dielectric constant $\varepsilon(x)$. In the "dispersive" design, the polychromatic input generates a spatially and wavelength dependent electric field complex amplitude $E(x, \lambda)$. A photodetector array probes the spatial field distribution and converts it into spectral information of the optical input via a linear transformation. Classical dispersive spectrometers using diffractive gratings, prisms, or resonant cavity arrays as the spectrum-splitting elements fall in this category[5-13]. Furthermore, the generalized "dispersive" spectrometers shown in Fig. 2a also encompass those based on the wavelength multiplexing principle, which date back to the static multi-slit design conceived by Golay in the 1940s[14] and have also garnered considerable interest recently[15-22]. The latter configuration illustrated in Fig. 2b applies a time-dependent modulation to the optical system such that its dielectric function $\varepsilon(x, t)$ is both spatially and temporally varying. Modulation of the dielectric function modifies the electric field distribution $E(\lambda, t)$ at the single-element detector,

from which the spectrum of incident light can be inferred through a linear transformation to map the light intensity values measured by the detector from the time domain to the spectral domain. Compared to the "dispersive" type spectrometers, properly designed time-domain "modulated" systems feature the Fellgett or multiplexing advantage, as the input light is concentrated on a single photodetector rather than being split between multiple detectors. As a result, the SNR is enhanced by a factor of square root N for the same integration time, where N is the number of spectral channels or data points[23]. Such time-domain modulation can be implemented via mechanical motion of optical components, for instance in the cases of FTIR spectrometers. Alternative modulation methods making use of electro-optic and thermo-optic effects have also been demonstrated[24-26].

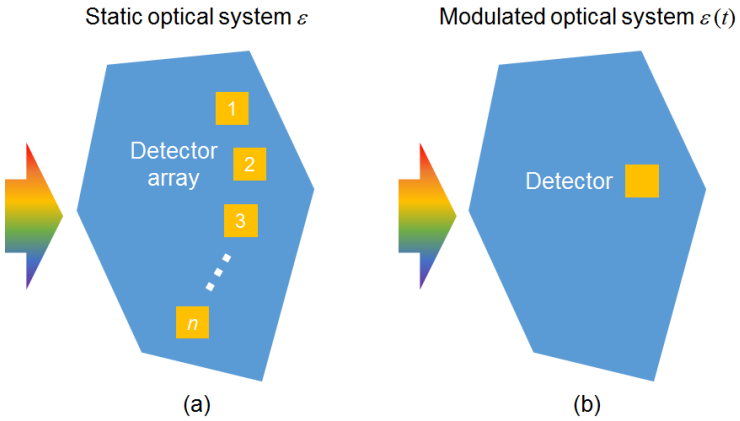

Fig. 2. Generic spectrometer models: a single mode polychromatic input is launched into an optical system and its spectral content is quantified via the detector output. In (a) the "dispersive" type configuration, the optical system is time-independent and a detector array is used to collect spatially "coded" spectral information; in (b) the "modulated" type design, the optical system is modulated and the resulting time-dependent single-element detector output is used to extract the spectral information.

Similar to laser-scanning systems, the detection limit of spectrometric sensors is also determined by the accessible optical path length in the sensing element. Spectral resolution $\delta\lambda$ (defined as the minimum resolvable wavelength difference) and bandwidth are two other important metrics.

Spectral resolution of both "dispersive" and "modulated" spectrometers scales inversely with the effective optical path length in the optical system. For optical systems with a deterministic optical path, the path length is proportional to the system linear dimension. For optical systems consisting of random scattering media, the effective path length scales with the square root of the system size[15]. It is therefore apparent that direct size down-scaling is not a preferred solution for spectrometer miniaturization and on-chip integration due to the deteriorating spectral resolution.

Spectral bandwidth of spectrometers, in general, equals the product of the number of spectral channels N and the spectral resolution $\delta\lambda$. Here N can also be interpreted as the number of useful detector elements in the "dispersive" configuration or distinctive optical states $\varepsilon(x, t)$ in the "modulated" scheme. In practice, the spectrometer bandwidth is often constrained by light source bandwidth or single-mode condition of the photonic components used to construct the spectrometer.

3. CHIP-SCALE OPTICAL CAVITY-ENHANCED PHOTOTHERMAL SPECTROSCOPY

The sensitivity of on-chip cavity-enhanced sensors is fundamentally limited by high waveguide losses as we discussed in Section II. Traditional on-chip microcavity absorption spectrometers measure the change in complex refractive index, the sensitivity of which is largely limited by scattering loss from cavity sidewall roughness[27-32]. In order to achieve sensitivities comparable to state-of-the-art benchtop spectroscopy instruments, on-chip sensors must exploit unique properties of their reduced size and waveguiding materials. In this section, we describe a method of performing photothermal spectroscopy to detect trace gases at the part-per-billion level (ppb). Photothermal spectroscopy has been predicted as a technique 10^4 times more sensitive than conventional microcavity absorption spectroscopy[33,34]. We propose a new technique that monitors the shift in cavity resonance as a result of heating. Resonant absorption of cavity light by the gas molecules thermally heats the cavity, producing a large resonant shift in a suitably designed microdisk cavity.

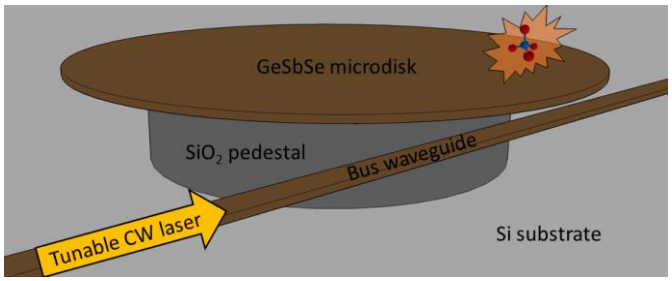

Fig. 3. Schematic of a suspended microdisk cavity structure for sensing a target gas molecule in the surrounding air. Brown denotes a 30 μm radius $Ge_{23}Sb_7Se_{70}$ microdisk coupled to a bus waveguide, all suspended 10 μm above a Si substrate by SiO_2 supports.

As a starting point, we consider a microdisk such as the one shown in Fig. 3 coupled to a bus waveguide that delivers light of wavelength λ_p and power I into the cavity. Input light launched into the bus waveguide with a coupling efficiency η and is scanned from low to high wavelength. When λ_p scans across a cavity resonance from short to long wavelengths, the cavity begins to heat, inducing a red shift in the cavity resonance assuming a positive thermo-optic coefficient. Maximum power is coupled into the cavity when the pump wavelength λ_p is equal to the heated-cavity resonance:

$$\lambda_{p,min} = \lambda_0 \left(1 + a\Delta T\right), \tag{1}$$

where λ_0 is the cold-cavity resonant wavelength and $a = \frac{1}{n_g}\frac{dn_{eff}}{dT} + a_L$ describes the shift in resonance due to thermal expansion (a_L) and index change. Continuing to scan the pump wavelength past this point results in less cavity heating and a subsequent blue-shift of the cavity resonance. The system relaxes to its off-resonant cold-cavity state at a rate equal to the system's thermal relaxation time. The change in transmission minima, or $\lambda_{p,min}$, is related to the absorption coefficient and absorption cross-section of the gas molecules as shown in the following analysis. We would like to note that a full description of the microcavity stability criterion was fully analyzed by Carmon, *et al.*[35], and is the basis for our analysis[36].

Here we fully describe a prototypical design of a photothermal gas sensor, numerically compute its sensitivity, and compare the numerical results with the analytical model described in our previous work[36]. Here we use HF gas as the

target analyte, which has strong absorption lines in the 2.4-2.5 μm region[37]. The modeling approach is however generic and can be readily adapted to photothermal sensors operating on other wavelengths.

The sensor geometry is a pedestal microdisk cavity with 60 μm diameter, as shown in Fig. 3. The cavity is fabricated from a high-index chalcogenide glass material for its low thermal conductivity and high photothermal figure of merit. Specifically, we will consider $Ge_{23}Sb_7Se_{70}$ which has a high index (n = 2.6 at 2.5 μm), is transparent between 1 and 15 μm wavelengths, and has a low thermal conductivity of 0.22 W/mK[38]. In the following, we only consider the effects of index change, such that $a = \frac{1}{n_g}\frac{dn_{eff}}{dT}$. For materials of positive thermal expansion coefficients, such as GeSbSe, the sensitivity will only be further enhanced by incorporating effects of volumetric thermal expansion. The chalcogenide glass cavity can be fabricated by thermal evaporation and lithographic patterning can be achieved by liftoff or reactive-ion etching. The cavity is air-clad to decrease thermal conductance and supported by the 10 μm tall SiO_2 pedestal with radius of 20 μm on a Si substrate.

To model the steady-state thermal properties of this system, we constructed a radially symmetric pedestal microdisk structure using the COMSOL Multiphysics package at room temperature with a 10 cm/s airflow. Next, we assumed a heat source with input power p_{int} and p_{ext} for the mode regions inside and outside the disk core as shown in Fig. 4a.

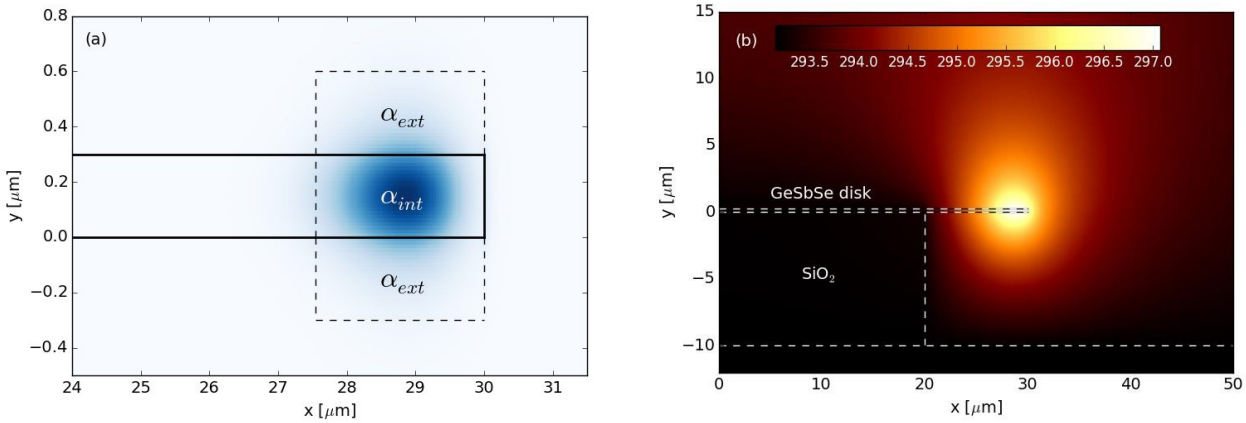

Fig. 4. (a) Cross-sectional profile of $|E|^2$ for the resonant cavity mode. (b) Steady state temperature profile in Kelvin of microdisk resonator for an intrinsic absorption of $\alpha_{int} = 10^{-4}$ cm^{-1}, external absorption of $\alpha_{ext} = 10^{-5}$ cm^{-1}, scattering loss of $\alpha_s = 0.023$ cm^{-1} and 10 mW input power in the cavity.

The scattering absorption coefficient was taken to be 0.1 dB/cm (0.023 cm^{-1}), which represents a microdisk cavity of $Q \sim 10^6$, consistent with our recent report of high-Q chalcogenide glass micro-resonators[40,41]. The internal absorption coefficient and in-coupled power $I\eta$ were varied as a function of external absorption coefficient to determine the sensitivity of the photothermal sensor. The cross-section of the steady-state thermal distribution was interpolated to fit the same mesh from the mode calculations (performed using Lumerical FDTD). The shift in resonant frequency as a function of this temperature rise was computed using first-order cavity perturbation theory.

Finally, the gas concentration detection limit is estimated from the HF absorption cross section at 2.45 μm, 7×10^{-18} cm^2/molecule[42] and assuming that system temperature fluctuations of ΔT_{res} = 0.1 °C·Hz$^{1/2}$ set the lower limit for wavelength resolution.

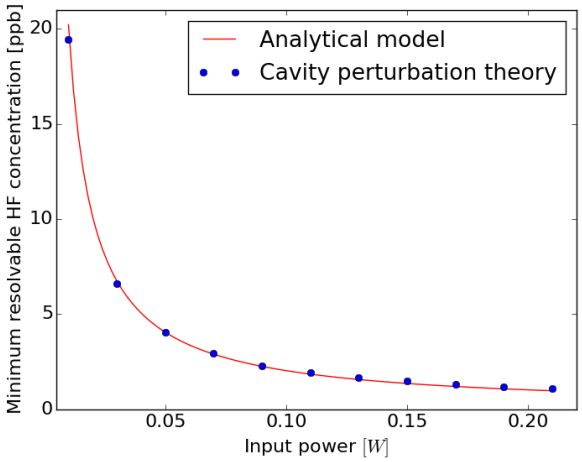

Fig. 5. Minimum resolvable concentration of HF gas molecules given as a function of the input power ($I\eta$) in the cavity given by the analytical model[36] (red) and from cavity perturbation theory (blue).

The results of these computations are shown in Fig. 5 for varying power and intrinsic absorption coefficients. We note that the main approximation made in the cavity perturbation theory results is the box-shaped heat sources. However, we anticipate this approximation to be small, since the temperature profile is relatively slow varying compared to the electromagnetic mode profile, as shown in Fig. 4b. From these results, we can see that the analytical expression for photothermal sensitivity[36] accurately predicts the power-dependence of the sensor. At modest input powers, detection on the 10's of ppb level is readily attainable.

In the above analysis, we have demonstrated that monitoring cavity heating as a result of resonant absorption from gas molecules is a viable method of ultrasensitive chemical detection. With modest design parameters and a microcavity designed for maximum thermal isolation, we have demonstrated the feasibility for on-chip gas sensing at a level comparable to the most sensitive free space optical sensors such as Herriott cells. By taking advantage of unique system and material properties at chip-scale dimensions (such as high thermal confinement and large thermo-optic coefficients), it is possible to circumvent large sensitivity penalties that arise from device down-sizing in traditional microcavity spectrometers.

5. DIGITAL FOURIER TRANSFORM INFRARED SPECTROSCOPY

As discussed in Section 2, the "modulated" type spectrometers claim the Fellgett advantage, which underlies their significantly improved SNR over that of the "dispersive" type instruments. The "modulated" type spectrometers are therefore better suited for infrared spectroscopy, as infrared detectors generally exhibit much inferior SNR compared to their counterparts operating at visible wavelengths (in particular, Si photodiodes). Furthermore, the "modulated" type

spectrometers can operate with single-element detectors, which is a far more cost-effective option than linear arrays or 2-D imaging arrays required for dispersive spectrometers.

FTIR is perhaps the most common "modulated" type of spectroscopic technique. The basic configuration of an FTIR spectrometer consists of an interferometer with one arm of variable optical path length. According to the Rayleigh criterion, the spectral resolution of an FTIR spectrometer is determined by the path length change ΔL of the variable arm:

$$\delta\nu = \frac{1}{\Delta L} \tag{2}$$

in wave numbers or:

$$\delta\lambda = \frac{\lambda^2}{\Delta L} \tag{3}$$

in wavelength, where λ is the center wavelength. Both (2) and (3) are consistent with our general conclusion that the spectral resolution of "modulated" type spectrometers is inversely proportional to the modulation amplitude.

In conventional FTIR spectrometers, the optical path length modulation is achieved by using movable mirrors. The use of mechanical moving parts compromises the robustness of conventional FTIR systems. Efforts to create on-chip FTIR spectrometers have thus far focused on either direct miniaturization of conventional systems using micro-electromechanical system (MEMS) technologies[43], or tunable Mach-Zehnder Interferometers (MZI) based on electro-optic (EO) or thermo-optic (TO) effects[24-26]. Nevertheless, these devices exhibit much inferior performance compared to their conventional bulk counterparts due to the limited optical path length tuning range accessible on a chip. Table I compares the modulation efficiency of several optical path length modulation approaches, which is defined as the phase change (in radians) imparted on light wave per unit propagation length (in centimeters). Table 1 also lists the spectral resolution of a 1-cm long device near 1550 nm wavelength utilizing these modulation mechanisms calculated using (3).

Table 1. Comparison of optical path length modulation methods for on-chip Fourier Transform Infrared spectroscopy

Modulation mechanism	Modulation efficiency (rad/cm)	Spectral resolution $\delta\lambda$ (nm) for a 1 cm long device at λ = 1.55 μm
Carrier plasma dispersion[44]	13	N/A
Thermo-optic effect in Si[45]	433	22
Liquid crystal clad waveguide[46]	1,578	6.15
MEMS movable mirror	40,500	0.24
Modification of waveguide path	93,200	0.1

Here we propose a novel spectrometer technology, digital Fourier Transform InfraRed (dFTIR), to overcome the aforementioned spectral resolution limit facing current on-chip spectrometers. The proposed spectrometer structure consists of an interferometer whose arms comprise a series of cascaded optical switches connected by waveguides of varying lengths. Unlike prior on-chip spectrometers where the arm length is changed by tuning the waveguide effective index, our approach modifies the optical path through which light propagates using the cascaded switches. Direct

modification of the waveguide path is a far more effective approach for changing the optical path length than index modulation, as it is not bound by the small magnitude of index perturbation as is shown in Table I, thus enabling much improved spectral resolution.

The structure is illustrated in Fig. 6. Incident light entering the device is split into the two interferometer arms with optical switches to direct the light into an upper waveguide in the "UP" state or a lower waveguide in the "DOWN" state. The reference paths are shown in black in Fig. 6a, while longer or shorter paths are shown in red. Each path in red is different from the black paths by a power of 2 times ΔL (ΔL being a pre-defined path length difference). As a result of this design, each permutation of the optical switches being "UP" or "DOWN" results in a different difference in optical path length between the two arms. Therefore, if there are 6 total switches as shown in Fig. 6b, there are $2^6 = 64$ different interferometer configurations. Similarly, for j optical switches, the spectral channel number is:

$$N = 2^j, \tag{4}$$

and the spectral resolution in wavelength is given by:

$$\delta\lambda \sim \frac{1}{2^j} \cdot \frac{\lambda^2}{n_{eff} \cdot \Delta L}, \tag{5}$$

where n_{eff} denotes the waveguide modal effective index. The spectral bandwidth in the wavelength domain is:

$$BW = \delta\lambda \cdot N \sim \frac{\lambda^2}{n_{eff} \cdot \Delta L}. \tag{6}$$

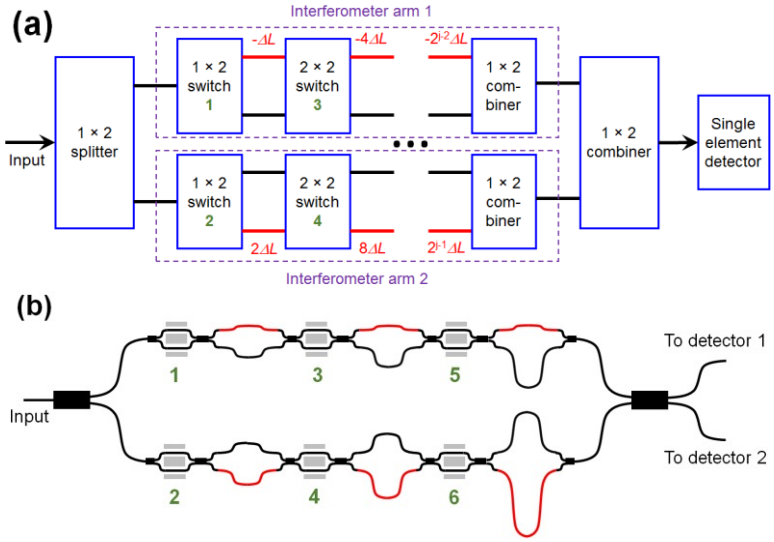

Fig. 6. (a) Block diagram of the dFTIR spectrometer design; (b) schematic layout of a 64-channel dFTIR spectrometer: the waveguide segments of varying lengths different from the standard length are shown in red (not drawn to scale). The green numbers label the 1 × 2 or 2 × 2 switches.

The equations suggest that performance scaling of the spectrometer can be readily achieved by increasing the number of switches j. To investigate the scaling behavior of the spectrometer, we consider an exemplary dFTIR device comprised of ridge waveguides and a total of j thermo-optic switches, both fabricated in a silicon-on-insulator (SOI) platform. Key performance specifications of SOI photonic components assumed in this analysis are quoted for devices processed in

commercial multi-project-wafer (MPW) runs, which are representative of state-of-the-art photonic manufacturing in a production-relevant setting[47-49]. To obtain sub-nm spectral resolution, the maximum path length difference between the two interferometer arms $2^j \cdot \Delta L$ should be in the order of several millimeters or more. Therefore, the thermo-optic switches and the splitters/combiners have negligible contributions to the overall device footprint. Each set of two optical switches, such as 1 and 2 in Fig. 6b, form a "stage". The black reference arms in each "stage" are constrained by the condition that the shorter arm lengths (the red paths labeled with negative numbers) have to be greater than zero. Now we examine a specific example of an on-chip spectrum analyzer covering the entire C and L bands (1530 – 1625 nm wavelengths). Here we use n_{eff} = 2.55, λ = 1577.5 nm, and ΔL = 10.3 μm. Fig. 7 plots the performance projections of the spectrometer. Taking j = 12, our calculations yield BW = 95 nm, $\delta\lambda$ = 0.023 nm, IL = 5.8 dB, and L_{tot} = 1.6 cm. These performance specifications are superior compared to commercial C/L band optical channel monitors[50]. Additionally, the waveguides in the interferometer arms can be folded into a zig-zag or spiral pattern to reduce the device footprint if necessary.

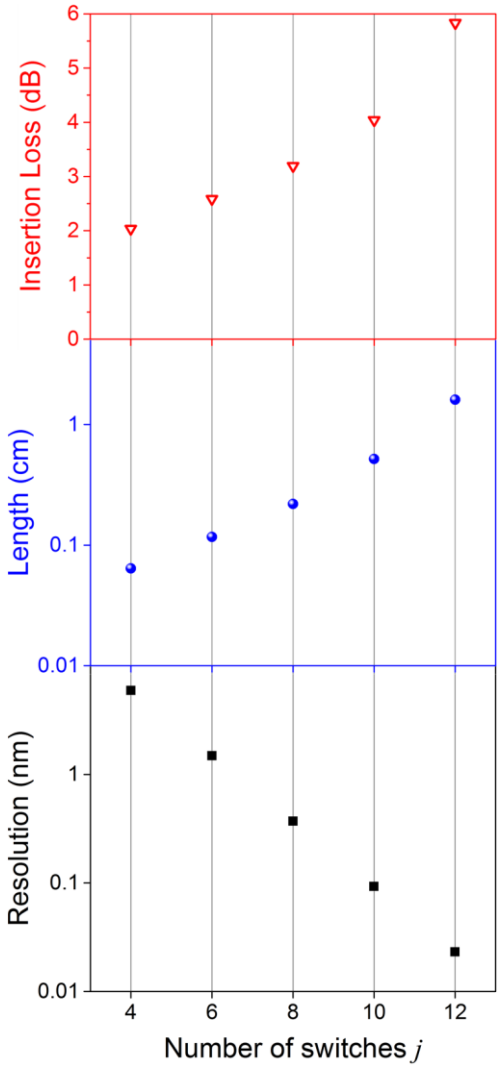

Fig. 7. Projected spectral resolution, interferometer arm length and insertion loss of the dFTIR spectrometer

Last but not least, it is also worth noting that the spectrometer design is highly tolerant against fabrication errors such as component cross-sectional dimension or length deviations. To counter such fabrication errors, a calibration step can be performed prior to using the device for spectroscopic interrogations. Calibration data will assume the form of a $2^j \times 2^j$ matrix. Each column of the matrix gives the transmittance through the spectrometer at different switch "UP"/"DOWN" state combinations, whereas each row of the matrix specifies the device transmittance at a particular "UP"/"DOWN" state configuration of the switches. The spectrograph of an arbitrary polychromatic input can be solved by recording the transmittance at all 2^j distinctive combinations of the switch "UP"/"DOWN" states, and multiplying the resulting vector with the inverse of the calibration matrix. For the same reason, operation bandwidth of the spectrometer is only limited by the single mode condition of the waveguides comprising the spectrometer rather than the operation bandwidth of the optical switches or the beam splitters/combiners, as high contrast ratio of the switches is *not* required to solve the spectrograph once the calibration matrix is measured. We further note that the calibration matrix is invariant for a given spectrometer device and therefore the calibration step only needs to be carried out once, and the calibration data can be stored for subsequent measurements.

6. SUMMARY

In this paper, we highlighted the challenges associated with on-chip integration of infrared spectroscopic sensors, in particular, performance penalties resulting from device size down-scaling. To resolve these challenges, we discussed two sensor designs uniquely capable of reaping performance benefits from scaling. In the first example, tight optical and thermal confinement in microphotonic devices lead to a gigantic photothermal sensitivity boost compared to the sensitivity of traditional absorption spectroscopic sensors. In the second case, we proposed a new on-chip Fourier Transform InfraRed spectrometer design leveraging two functions made available in compact, chip-scale platforms through photonic integration: optical switching and long, folded optical paths. In both cases we have shown that on-chip spectroscopic sensors can attain performance metrics comparable to or even superior to conventional bulk optical instruments.

7. ACKNOWLEDGEMENT

This work was supported in part by NSF award 1506605 and DOE NNSA grant DE-NA0002509.

REFERENCES

[1]B. Stuart, *Infrared spectroscopy*, John Wiley & Sons, Inc., 2005.

[2]G. Overton, "How spectrometers have shrunk and grown since 2010," *Laser Focus World*, vol. 52, no. 2, pp. 35-41, Feb. 2016.

[3]S. Sharpe, T. Johnson, R. Sams, P. Chu, G. Rhoderick, and P. Johnson, "Gas-phase databases for quantitative infrared spectroscopy," *Appl. spectrosc.*, vol. 58, pp. 1452-1461, 2004.

[4]D. Herriott, and H. Schulte, "Folded optical delay lines," *Appl. Opt.*, vol. 4, pp. 883-889, 1965.

[5]A. Subramanian, E. Ryckeboer, A. Dhakal, F. Peyskens, A. Malik, B. Kuyken, H. Zhao, S. Pathak, A. Ruocco, A. De

Groote, P. Wuytens, D. Martens, F. Leo, W. Xie, U. Dave, M. Muneeb, P. Van Dorpe, J. Van Campenhout, W. Bogaerts, P. Bienstman, N. Le Thomas, D. Van Thourhout, Z. Hens, G. Roelkens, and R. Baets, "Silicon and silicon nitride photonic circuits for spectroscopic sensing on-a-chip [Invited]," *Photon. Res.*, vol. 3, pp. B47-B59, 2015.

[6]W. Bogaerts, S. Selvaraja, P. Dumon, J. Brouckaert, K. De Vos, D. Van Thourhout, and R. Baets, "Silicon-on-insulator spectral filters fabricated with CMOS technology," *IEEE J. Sel. Top. Quantum Electron.*, vol. 16, pp. 33-44, 2010.

[7]G. Roelkens, U. Dave, A. Gassenq, N. Hattasan, C. Hu, B. Kuyken, F. Leo, A. Malik, M. Muneeb, E. Ryckeboer, S. Uvin, Z. Hens, R. Baets, Y. Shimura, F. Gencarelli, B. Vincent, R. Loo, J. Van Campenhout, L. Cerutti, J. Rodriguez, E. Tournié, X. Chen, M. Nedeljkovic, G. Mashanovich, L. Shen, N. Healy, A. Peacock, X. Liu, R. Osgood, and W. Green, "Silicon-based heterogeneous photonic integrated circuits for the mid-infrared," *Opt. Mater. Express*, vol. 3, pp. 1523-1536, 2013.

[8]S. Babin, A. Bugrov, S. Cabrini, S. Dhuey, A. Goltsov, I. Ivonin, E. Kley, C. Peroz, H. Schmidt, and V. Yankov, "Digital optical spectrometer-on-chip," *Appl. Phys. Lett.*, vol. 95, pp. 041105, 2009.

[9]M. Florjańczyk, P. Cheben, S. Janz, A. Scott, B. Solheim, and D. Xu, "Multiaperture planar waveguide spectrometer formed by arrayed Mach-Zehnder interferometers," *Opt. Express*, vol. 15, pp. 18176-18189, 2007.

[10]Z. Xia, A. Eftekhar, M. Soltani, B. Momeni, Q. Li, M. Chamanzar, S. Yegnanarayanan, and A. Adibi, "High resolution on-chip spectroscopy based on miniaturized microdonut resonators," *Opt. Express*, vol. 19, pp. 12356-12364, 2011.

[11]F. Civitci, M. Hammer, and H. Hoekstra, "Planar prism spectrometer based on adiabatically connected waveguiding slabs," *Opt. Commun.*, vol. 365, pp. 29-37, 2016.

[12]R. DeCorby, N. Ponnampalam, E. Epp, T. Allen, and J. McMullin, "Chip-scale spectrometry based on tapered hollow Bragg waveguides," *Opt. Express*, vol. 17, pp. 16632-16645, 2009.

[13]X. Gan, N. Pervez, I. Kymissis, F. Hatami, and D. Englund, "A high-resolution spectrometer based on a compact planar two dimensional photonic crystal cavity array," *Appl. Phys. Lett.*, vol. 100, pp. 231104, 2012.

[14]M. Golay, "Multi-Slit Spectrometry," *J. Opt. Soc. Am. A*, vol. 39, pp. 437-444, 1949.

[15]B. Redding, S. Liew, R. Sarma, and H. Cao, "Compact spectrometer based on a disordered photonic chip," *Nat. Photonics*, vol. 7, pp. 746-751 (2013).

[16]N. Wan, F. Meng, T. Schröder, R. Shiue, E. Chen, and D. Englund, "High-resolution optical spectroscopy using multimode interference in a compact tapered fibre," *Nat. Commun.*, vol. 6, pp. 7762, 2015.

[17]J. Bao, and M. Bawendi, "A colloidal quantum dot spectrometer," *Nature*, vol. 523, pp. 67-70, 2015.

[18]E. le Coarer, S. Blaize, P. Benech, I. Stefanon, A. Morand, G. Lérondel, G. Leblond, P. Kern, J. M. Fedeli, and P. Royer, "Wavelength-scale stationary-wave integrated Fourier-transform spectrometry," *Nat. Photonics*, vol. 1, pp. 473-478, 2007.

[19]B. Redding, S. Popoff, and H. Cao, "All-fiber spectrometer based on speckle pattern reconstruction," *Opt. Express*, vol. 21, pp. 6584-6600, 2013.

[20]B. Redding and H. Cao, "Using a multimode fiber as a high-resolution, low-loss spectrometer," *Opt. Lett.*, vol. 37, pp. 3384-3386, 2012.

[21]M. Gehm, S. McCain, N. Pitsianis, D. Brady, P. Potuluri, and M. Sullivan, "Static two-dimensional aperture coding for multimodal, multiplex spectroscopy," *Appl. Opt.*, vol. 45, pp. 2965-2974, 2006.

[22]Z. Xu, Z. Wang, M. Sullivan, D. Brady, S. Foulger, and A. Adibi, "Multimodal multiplex spectroscopy using photonic crystals," *Opt. Express*, vol. 11, pp. 2126-2133, 2003.

[23]R. Sellar and G. Boreman, "Comparison of relative signal-to-noise ratios of different classes of imaging spectrometer," *Appl. Opt.*, vol. 44, pp. 1614-1624, 2005.

[24]T.-H. Chao, T. T. Lu, S. R. Davis, S. D. Rommel, G. Farca, B. Luey, A. Martin, and M. H. Anderson, “Compact liquid crystal waveguide based Fourier transform spectrometer for in-situ and remote gas and chemical sensing,” *Proc. SPIE*, vol. 6977, pp. 69770P-11, 2008.

[25]B. Dong, H. Cai, Y. Gu, Z. Yang, Y. Jin, Y. Hao, D. Kwong, and A. LIU, "Nano-Silicon-Photonic Fourier Transform Infrared (FTIR) Spectrometer-on-a-Chip," in CLEO: 2015, OSA Technical Digest (online) (Optical Society of America, 2015), paper STu4I.1.

[26]Y. Dattner, and O. Yadid-Pecht, “Fully integrated complementary metal oxide semiconductor (CMOS) Fourier transform infrared (FTIR) spectrometer and raman spectrometer,” U.S. Patent Application 2013/0321816 A1, Dec. 5, 2013.

[27]Y. Chen, H. Lin, J. Hu, and M. Li, “Heterogeneously integrated silicon photonics for the mid-infrared and spectroscopic sensing,” *ACS Nano*, vol. 8, pp. 6955-6961, 2014.

[28]J. Hu, N. Carlie, L. Petit, A. Agarwal, K. Richardson, and L. C. Kimerling, “Cavity-enhanced infrared absorption in planar chalcogenide glass resonators: experiment & analysis,” *J. Lightwave Technol.*, vol. 27, pp. 5240-5245, 2009.

[29]C. Smith, R. Shankar, M. Laderer, M. Frish, M. Loncar, and M. Allen, "Sensing nitrous oxide with QCL-coupled silicon-on-sapphire ring resonators," *Opt. Express*, vol. 23, pp. 5491-5499, 2015.

[30]A. Nitkowski, L. Chen, and M. Lipson, "Cavity-enhanced on-chip absorption spectroscopy using microring resonators," *Opt. Express*, vol. 16, pp. 11930-11936, 2008.

[31]A. Nitkowski, A. Baeumner, and M. Lipson, "On-chip spectrophotometry for bioanalysis using microring resonators," *Biomed. Opt. Express*, vol. 2, pp. 271-277, 2011.

[32]V. Singh, P. Lin, N. Patel, H. Lin, L. Li, Y. Zou, F. Deng, C. Ni, J. Hu, J. Giammarco, A. P. Soliani, B. Zdyrko, I. Luzinov, S. Novak, J. Novak, P. Wachtel, S. Danto, J. D. Musgraves, K. Richardson, L. C. Kimerling, and A. Agarwal, "Mid-infrared materials and devices on a Si platform for optical sensing," *Sci. Tech. Adv. Mater.*, vol. 15, pp. 014603, 2014.

[33]J. Hu, “Ultra-sensitive chemical vapor detection using micro-cavity photothermal spectroscopy,” *Opt. Express*, vol. 18, pp. 22174-22186, 2010.

[34]H. Lin, Y. Zou, and J. Hu, "Double resonance 1-D photonic crystal cavities for single-molecule mid-infrared photothermal spectroscopy: theory and design," *Opt. Lett.*, Vol. 37, pp. 1304-1306, 2012.

[35]T. Carmon, L. Yang, and K. Vahala, "Dynamical thermal behavior and thermal self-stability of microcavities," *Opt. Express*, vol. 12, pp. 4742-4750, 2004.

[36]D. Kita, H. Lin, A. Agarwal, K. Richardson, I. Luzinov, T. Gu, and J. Hu, "On-chip infrared spectroscopic sensing: redefining the benefits of scaling," *IEEE J. Sel. Top. Quantum Electron.*, vol. 23, pp. 5900110, 2017.

[37]W. Herget, W. Deeds, N. Gailar, R. Lovell, and A. Nielsen, "Infrared Spectrum of Hydrogen Fluoride: Line Positions and Line Shapes. Part II. Treatment of Data and Results," *J. Opt. Soc. Am.*, vol. 52, pp. 1113-1119, 1962.

[38]L. Petit, N. Carlie, H. Chen, S. Gaylord, J. Massera, K. Richardson, G. Boudebs, J. Hu, A. Agarwal, and L. C. Kimerling, “Compositional dependence of the nonlinear refractive index of new germanium-based chalcogenide glasses,” *J. Solid State Chem.*, vol. 182, pp. 2756-2761, 2009.

[39]J. Robinson, K. Preston, O. Painter, and M. Lipson, "First-principle derivation of gain in high-index-contrast waveguides," *Opt. Express*, vol. 16, pp. 16659-16669, 2008.

[40]Q. Du, Y. Huang, J. Li, D. Kita, J. Michon, H. Lin, L. Li, S. Novak, K. Richardson, W. Zhang and J. Hu, “Low loss photonic devices in Ge-Sb-S chalcogenide glass,” *Opt. Lett.*, vol. 41, pp. 3090-3093, 2016.

[41]K. Richardson, L. Petit, N. Carlie, B. Zdyrko, I. Luzinov, J. Hu, A. Agarwal, L. C. Kimerling, T. Anderson, and M. Richardson, “Progress on the fabrication of on-chip, integrated chalcogenide glass (ChG)-based sensors,” *J. Nonlinear Opt. Phys. Mater.*, vol. 19, pp. 75-99, 2010.

[42]VPL Molecular Spectroscopic Database, available at: http://vpl.astro.washington.edu/spectra/hf.htm

[43]L. P. Schuler, J. S. Milne, J. M. Dell and L. Faraone, "MEMS-based microspectormeter technologies for NIR and MIR wavelengths," *J. Phys. D, Appl. Phys.*, vol. 42, pp. 133001, 2009.

[44]H. Xu, X. Xiao, X. Li, Y. Hu, Z. Li, T. Chu, Y. Yu, and J. Yu, “High speed silicon Mach-Zehnder modulator based on interleaved PN junctions,” *Opt. Express*, vol. 20, pp. 15093-15099, 2012.

[45]N. Harris, Y. Ma, J. Mower, T. Baehr-Jones, D. Englund, M. Hochberg, and C. Galland, "Efficient, compact and low loss thermo-optic phase shifter in silicon," *Opt. Express*, vol. 22, pp. 10487-10493, 2014.

[46]T. Ako, A. Hope, T. Nguyen, A. Mitchell, W. Bogaerts, K. Neyts, and J. Beeckman, "Electrically tuneable lateral leakage loss in liquid crystal clad shallow-etched silicon waveguides," *Opt. Express*, vol. 23, pp. 2846-2856, 2015.

[47]T. Baehr-Jones, “OpSIS-IME OI50 Process – Performance Summary,” Available at: http://opsisfoundry.org/wp-content/uploads/opsis_oi50_performance_summary_10_8_13.pdf

[48]Y. Zhang, S. Yang, A. Lim, G. Lo, C. Galland, T. Baehr-Jones, and M. Hochberg, "A compact and low loss Y-junction for submicron silicon waveguide," *Opt. Express*, vol. 21, pp. 1310-1316, 2013.

[49]P. Dumais, Y. Wei, M. Li, F. Zhao, X. Tu, J. Jiang, D. Celo, D. Goodwill, H. Fu, D. Geng, and e. Bernier, "2x2 Multimode Interference Coupler with Low Loss Using 248 nm Photolithography," in Optical Fiber Communication Conference, OSA Technical Digest (online) (Optical Society of America, 2016), paper W2A.19.

[50]“Optical Channel Monitor Based On Planar Lightwave Circuit Technology,” Available at: http://www.enablence.com/technologies/wp-content/uploads/2013/07/Datasheet_OCSD_OCM_PLC.pdf